RSC Advances

PAPER

View Article Online
View Journal | View Issue



Cite this: *RSC Adv.*, 2023, **13**, 12670

# Synergism between hierarchical MFI zeolites and alumina in alkene cross-metathesis reactions as a function of composition†

Ning Wei,[abc] Weiping Zhang, *[c] Dazhi Zhang[a] and Shengjun Huang *[a]

Synergism between hierarchical zeolites and alumina in the preparation of active Mo catalysts, as a function of composition ratios, has been demonstrated in the cross-metathesis reaction between ethene and 2-butene. The metathesis reaction activity, reflected by ethene conversion, increases from 24.1% to 49.2% with the increase in the alumina content in composites from 10 wt% to 30 wt%. A further increase in the alumina content leads to the reduction in the metathesis activity, in which the ethene conversion decreases from 30.3% to 4.8% upon the enhanced alumina content from 50 wt% to 90 wt%. The impact of alumina content on the metathesis activity is closely associated with the interaction mode between the hierarchical ZSM-5 zeolite and alumina. TEM observation as well as EDS analysis and XPS results prove the progressive coating of alumina phase on the surface of zeolites along with the progressive enhancement of alumina content. The moderate alumina content in the composite enables the desired interaction between hierarchical zeolites and alumina, which is beneficial for the preparation of active catalysts for the alkene cross-metathesis reaction.

Received 13th March 2023
Accepted 10th April 2023

DOI: 10.1039/d3ra01642k

rsc.li/rsc-advances



## Introduction

Zeolite-based catalysts have been extensively employed in various industrial processes such as catalytic cracking, alkylation, and isomerization.[1–6] In general, the shaping of zeolites into a technical body by the addition of binders (for instance, alumina) is essential to meet the overall imperatives for the smooth running of these processes.[7] Initially, the binder component is often regarded as an inert phase, which mainly contributes to the improvement in mechanical strength and the modification in thermal and mass transfer properties. Owing to the innovation of characterization techniques for the industrial relevant catalysts, functionality-performance relationships within the composite catalysts are acquired beyond the mixing and physical effects.[8–13]

Recent exemplary publications report consequences of the location of metallic active species or distribution of zeolite and binder on the specific reactions.[14–18] The interaction of zeolites with binders has significant impacts on the entrapment of specific poisons, modification of deactivation behaviours and neutralization of Brønsted acid sites.[10,19,20] In the case of zeolite composites supported metal oxides/supported metal catalysts, the primary issue is the competition or preferential distribution of metal/metal oxides on the composite supports. Given the discrepancy between zeolites and binders (*e.g.* alumina), the concurrent exposure of zeolite-binder composites to the active metal precursor complicates the distribution/location and heterogeneity degree of the metal species. The distribution of metal species can be tailored by the specific preparation procedure.[21,22] For instance, the deposition of Pt on $\gamma$-$Al_2O_3$ leads to a nanoscale intimacy between Pt sites and acid sites on zeolites, which is beneficial for the hydro-isomerization activity of bifunctional catalysts.[14,15,22] On the other hand, the location/distribution of metal/metal oxides in zeolite composite-supported catalysts is also influenced by the interaction mode between zeolites and binders.[8,23] In particular, the investigation of the interaction mode between zeolites and binders is necessary for the design and optimization of zeolite composite catalysts.

Our previous investigation disclosed the synergetic effect between zeolites and alumina for the preparation of active catalysts for alkene cross-metathesis reaction,[8,24] which plays an important role in the tuning of product outputs of alkenes. We have developed several $MoO_3$/zeolite–alumina and $WO_3$/zeolite–alumina composite catalysts for the alkene cross-metathesis reaction under mild conditions, in which alumina plays as the disperser of surface species and the zeolite plays as the anchorages for active sites, respectively.[8,24–27] In the past, it was found that the topology of zeolites for the preparation of active composite catalysts for olefin metathesis is limited to BEA, MOR and FAU. The microporous MFI zeolite cannot be used for the

[a]*Division of Fossil Energy Conversion, Dalian Institute of Chemical Physics, Chinese Academy of Sciences, Dalian, 116023, China. E-mail: huangsj@dicp.ac.cn*
[b]*University of Chinese Academy of Sciences, Beijing 100049, China*
[c]*State Key Laboratory of Fine Chemicals, School of Chemical Engineering, Dalian University of Technology, Dalian 116024, China. E-mail: wpzhang@dlut.edu.cn*

† Electronic supplementary information (ESI) available. See DOI: https://doi.org/10.1039/d3ra01642k

preparation of active metathesis catalysts. Our recent investigation has demonstrated that the introduction of intracrystalline mesoporosity to MFI zeolites enables the achievement of active metathesis catalysts. The infilling of alumina slices into zeolite intracrystalline mesopores for the creation of intrazeolite–alumina interface along the zeolite intracrystalline mesopore has been disclosed as the desirable interaction mode between hierarchical zeolites and alumina, which enables the evolution of highly active $MoO_x$ sites.[28]

In this work, the synergetic effect between hierarchical ZSM-5 zeolites and alumina for the preparation of active Mo-based catalysts, as a function of composition, is demonstrated in the cross-metathesis reaction between ethene and 2-butene. Meanwhile, the metathesis activity of composite catalysts is closely associated with the alumina content in the composite supports. The ethene conversion increases from 24.1% to 49.2% with the increase in the alumina content in composites from 10 wt% to 30 wt%. A further increase in the alumina content leads to the reduction in the ethene conversion. Such impact of alumina content on the metathesis activity of catalysts is closely associated with the interaction mode between hierarchical zeolites and alumina. As reflected by the TEM observation as well as EDS analysis and XPS results, the zeolite is progressively coated and enveloped by the alumina phase with the enhanced alumina content in the composite supports. The desired interaction mode between hierarchical zeolites and alumina, as a result of moderate alumina content, accounts for the achievement of active metathesis catalysts.

## Experimental section

The preparation procedures of the hierarchical ZSM-5 zeolite–alumina composite supported Mo-based catalysts are shown in Scheme 1, and the preparation details are given as follows:

### Preparation of hierarchical MFI zeolites

Hierarchical ZSM-5 zeolites were prepared by treating pristine ZSM-5 zeolites (denoted as Z, commercially available from Shanghai Fuxu Zeolite Co., Ltd., protonic-form, Si/Al = 30.9) with aqueous solution of NaOH. Typically, the pristine zeolite powder (12 g) was charged into the aqueous NaOH solution (360 ml, 0.2 M NaOH) in a polypropylene bottle at 338 K with magnetic stirring. After 0.5 h, the alkaline-treated samples were collected by centrifugation, washed thoroughly with deionized water, dried overnight at 373 K and subsequently calcined at 823 K for 3 h. These samples were converted into the protonic form by three consecutive ammonium-exchange (0.8 M $NH_4Cl$) and sequential calcination at 823 K for 3 h. The obtained hierarchical MFI zeolite is designated as hZ.

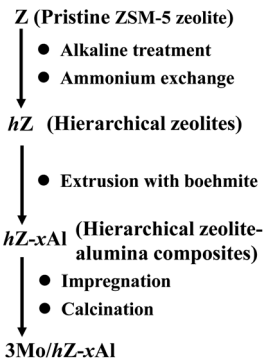


Scheme 1 Description for the preparation of 3Mo/hZ–*x*Al catalysts. hZ–*x*Al represents the composites of hZ–$Al_2O_3$, and *x* refers to the weight percent (wt%) of alumina in the composite supports.

### Preparation of hierarchical zeolite–alumina composite supports

The hierarchical zeolite–alumina composites were prepared by extruding a mixture of hierarchical zeolites (hZ) and boehmite powder (Fushun Petrochemical Industrial Co., Ltd.) using $HNO_3$ (65.0–68.0%, Xilong Scientific Co., Ltd.) as a peptizer agent and sesbania gum powder (Henan Jiujin Technology Co. Ltd.) as a lubricating agent. Typically, a mixture of hierarchical zeolites, boehmite and sesbania gum powder forms a paste by adding nitric acid solution (10 wt%), and subsequent extrusion in a homemade extruder equipped with a cylindrical die plate with the diameter of 3 mm. The drawn extrudate was left at room temperature overnight and placed in a muffle furnace at 393 K for 2 h. After calcination at 773 K for 2 h, the obtained extrudates were grounded into 20–40 mesh. The final hierarchical zeolite–alumina composites are denoted as hZ–*x*Al.

### Catalysts preparation

The catalysts with 3 wt% Mo loading were prepared by impregnating hierarchical zeolite–alumina composite supports with a desirable amount of ammonium hepta-molybdate (>99.0%, Sinopharm Group Chemical Reagent Co., Ltd.) solution according to the incipient wetness method. The impregnated samples were dried at 333 K overnight and subsequentially calcined in flowing air at 823 K for 3 h. The obtained catalysts are denoted as 3Mo/hZ–*x*Al.

### Preparation of comparative samples

The hierarchical zeolite (hZ) or gamma-alumina-supported Mo-based catalysts were prepared by an incipient wetness impregnation method. The impregnation procedures are the same as described above. The final catalysts are denoted as 3Mo/hZ and 3Mo/Al, respectively, in which Al represents $\gamma$-$Al_2O_3$.

### Characterization

The Mo content of samples was determined using a Philips Magix 601X X-ray fluorescence (XRF) spectrometer. $N_2$ adsorption measurements were carried out at 77 K using a Micromeritics ASAP-2460 analyzer. Prior to measurements, the samples were evacuated at 623 K for 10 h. Hydrogen temperature-programmed reduction ($H_2$-TPR) experiments were performed using a Micromeritics ASAP-2920 analyzer equipped with a TCD detector. The sample (300 mg) was purged at 823 K at a heating rate of 10 K $min^{-1}$ under helium flow for 30 min and then cooled to 373 K to remove the moisture.

Afterward, the sample was heated from 373 K to 1173 K at a heating rate of 14 K $min^{-1}$ under 10% $H_2$/Ar and kept at 1173 K until a stable signal (the engineers from Micromeritics note that the operating temperature of equipment should be below 1273 K). X-ray diffraction (XRD) patterns were obtained using an X'Pert Pro/PANalytical Diffractometer (Cu K$\alpha$ radiation, 40 kV, 40 mA) from 5° to 70° (2$\theta$) at a scanning rate of 7° $min^{-1}$. X-ray photoelectron spectroscopy (XPS) measurements were performed using a Thermo Scientific ESCALAB 250 XI spectrometer. The Al K$\alpha$ radiation (1486.6 eV) was used as the excitation source. The C 1s lines were used as the internal references (binding energy 284.8 eV) for calibrations. The transmission electron microscopy (TEM) observations were carried out using a JEOL JEM-2100 microscope. Energy-dispersive spectroscopy (EDS) analysis was also performed using this microscope equipped with an X-ray energy analyzer.

### Catalytic reactions

The cross-metathesis reaction between ethene and 2-butene was carried out on a continuous flowing fixed-bed reactor under atmospheric pressure. The reactor comprises the isomerization zone on the top of the middle and the metathesis zone on the bottom of the middle. The ZSM-5 based catalyst was used for the isomerization of 1-butene to 2-butene, which enables a stable composition (53 mol% ethene : 44 mol% 2-butene : 3 mol% 1-butene) for the sequential metathesis reaction. Both the isomerization catalyst (20–40 mesh, 2.8 g) and the metathesis catalyst (20–40 mesh, 1.0 g) were pretreated at 823 K for 1 h in a high-purity $N_2$ atmosphere to remove the moisture. After the reactor was cooled down to 383 K, the gas mixture of 1-butene/ethene (a molar ratio of 1/1) was introduced into a reactor with a weight hourly space velocity (WHSV) of 1.5 g $g^{-1}$ $h^{-1}$ (1-butene + ethene). The products were analyzed using an online gas chromatograph (Tianmei GC 7900) equipped with a SE-30 column and a flame ionization detector (FID). The catalytic performance was measured by the ethene conversion and the propene selectivity, which were calculated according to the following equations:

$$\text{Conversion of ethene} = \frac{N_{\text{in}}(C_2^=) - N_{\text{out}}(C_2^=)}{N_{\text{in}}(C_2^=)} \times 100\%$$

$$\text{Selectivity of propene} = \frac{N_{\text{out}}(C_3^=)}{\sum_m N_{\text{out}}(C_m^=)} \times 100\%$$

where $N_{\text{in}}(C_2^=)$ and $N_{\text{out}}(C_2^=)$ represent the molar amounts of ethene at the inlet and outlet of the reactor, respectively. $N_{\text{out}}(C_m^=)$ represents the molar amounts of products with certain carbon number, including propene ($C_3^=$), pentene ($C_5^=$), hexene ($C_6^=$) and heavy product (denoted as $C_{7+}^=$).

## Results and discussion

### Metathesis activity as a function of alumina content

Fig. 1 demonstrates the impacts of alumina content in the composite supports on the catalytic performance of 3Mo/hZ–$x$Al catalysts for the cross-metathesis reaction. A low ethene conversion around 24.1% is observed for 3Mo/hZ–10Al. The enhancement of alumina content to 30 wt% enables the maximum conversion of 49.2% over 3Mo/hZ–30Al catalysts. A further increment in the alumina content leads to a decrease in the metathesis activity. The ethene conversion decreases steeply to 30.3% for 3Mo/hZ–50Al, declines substantially to 10.9% for 3Mo/hZ–70Al and 4.8% for 3Mo/hZ–90Al, respectively. Analogous tendency can also be observed for the propene selectivity (Fig. S1 and Table S1†). As a sharp comparison, the poor metathesis activity has been observed for hierarchical zeolites or alumina-supported Mo-based catalysts, in which 3Mo/hZ and 3Mo/Al catalysts just give 0.8% and 2.1% ethene conversion, respectively (Table S1†). Such comparative results indicate the synergetic effect between hierarchical zeolites and alumina for the preparation of active metathesis catalysts as a function of alumina content.

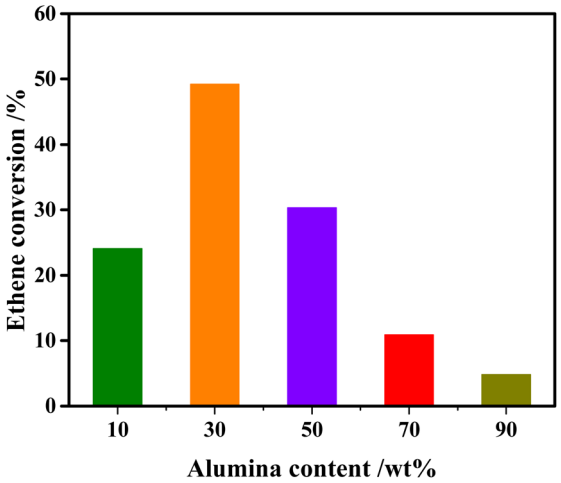


Fig. 1 Ethene conversion of 3Mo/hZ–$x$Al catalysts with different alumina contents. Reaction conditions: time on stream (TOS) = 4 h, $T$ = 383 K, $P$ = 0.1 MPa, WHSV = 1.5 g $g^{-1}$ $h^{-1}$ (feed composition of metathesis reaction: 53 mol% ethene, 44 mol% 2-butene and 3 mol% 1-butene), ethene/2-butene = 1.2 (molar ratio).

### Characterization of the crystalline and pore structure of composites

The XRD patterns of 3Mo/hZ–$x$Al catalysts are shown in Fig. 2. 3Mo/hZ and 3Mo/hZ–$x$Al catalysts show the characteristic peaks (2$\theta$ = 7.9°, 8.9°, 23.1°, 23.9° and 24.4°) of the ZSM-5 zeolite, demonstrating the preservation of the zeolite framework. The characteristic peaks of crystalline $MoO_3$ or $Al_2(MoO_4)_3$ are not discerned in the patterns of 3Mo/hZ–$x$Al catalysts, suggesting that the Mo-oxo species are well dispersed on the hierarchical zeolite–alumina composite supports.

The pore structure properties of hierarchical zeolite–alumina composite supports were determined by the $N_2$ adsorption–desorption isotherms and pore size distribution. As shown in Fig. 3, the hierarchical zeolite hZ gives a combined type I and IV isotherm with a small hysteresis loop in the relative pressure range of 0.45–0.9 and a typical mesopore size around 14 nm, indicating the created mesopore inside the MFI

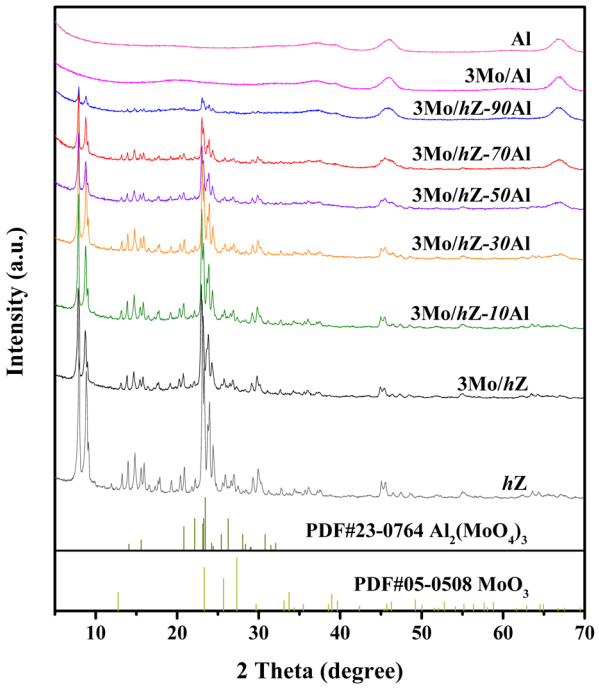


Fig. 2 XRD patterns of 3Mo/hZ–*x*Al catalysts with different alumina contents.

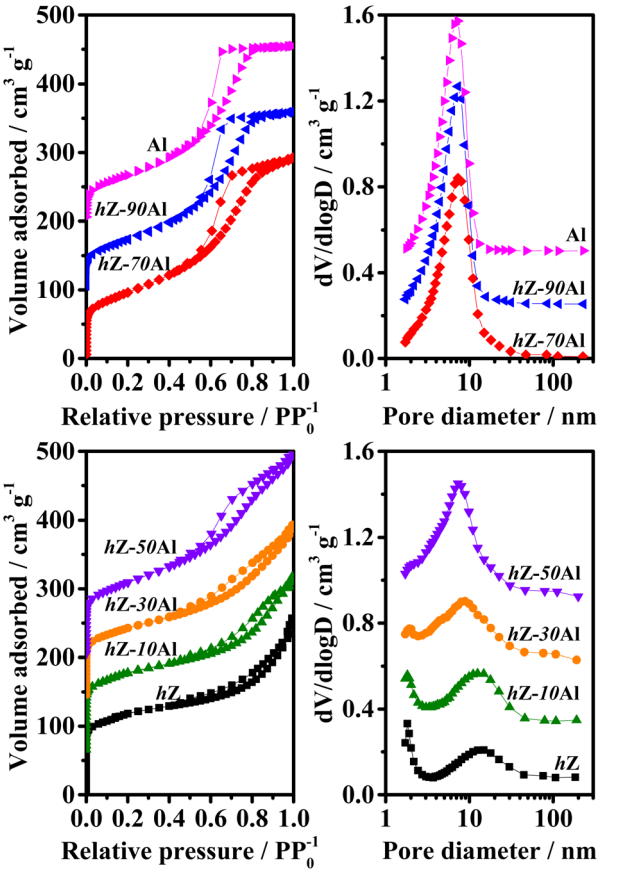


Fig. 3 $N_2$ adsorption–desorption isotherms of hZ–*x*Al composites with different alumina contents and Barrett–Joyner–Halenda pore size distribution derived from the adsorption branches of the isotherms.

zeolite by alkaline treatment. In the case of low/middle alumina content (10–30 wt%), the isotherm and mesopore size distribution of the composite support are close to those of hZ. As the alumina content increases, the isotherms and mesopore size distribution of composite supports steadily transform into the characters of alumina.

### Microscopic observations on the interaction mode between hierarchical zeolites and alumina

The TEM observation and EDS analysis provide a visual proof for the interaction mode between hierarchical zeolite and alumina, as a function of alumina content. As shown in Fig. 4a, the light patches are associated with the presence of zeolitic intracrystalline mesopore in the 3Mo/hZ–10Al catalysts. Meanwhile, dark zones (marked as a1 as an example) and bright zones (marked as a2 as an example) were observed on the surface of zeolites. The EDS spectra of a1 exhibited a higher Al concentration than that of a2 (Fig. 4d), indicating the presence of alumina coating on the surface of zeolite in the dark zones (a1).

Upon the enhancement of alumina content to 50 wt%, more dark zones are observed on the 3Mo/hZ–50Al catalysts. Meanwhile, the surface of hierarchical zeolites is enveloped partially by irregular alumina aggregates (Fig. 4b). The absence of the Si element in zone b1 further indicates that these aggregates are assigned to the alumina phase (Fig. 4e). A further increase in the alumina content to 70 wt% leads to the coating and enveloping of irregular alumina aggregates on the hierarchical zeolites, which is confirmed by the thick alumina aggregates on the external surface of hierarchical zeolite in zone c1 and high Al concentration in zone c2 (Fig. 4c and f). Therefore, the TEM observation and EDS analysis confirm the progressive coating and enveloping of alumina on the hierarchical zeolite along with the enhanced alumina content.

Such evolution in the interaction mode is further reflected by the alteration in the chemical environment of Si species. As shown in Fig. 5, the XPS Si 2p spectra of 3Mo/hZ show the characteristic peak of silicon sites in the zeolitic lattice with a binding energy around 103.8 eV.[29,30] Upon the introduction of alumina, the binding energy (BE) value of Si 2p downshifts to 103.6 eV for 3Mo/hZ–10Al, obvious reduction to 103.5 eV for 3Mo/hZ–30Al and 103.3 eV for 3Mo/hZ–50Al, respectively. Such downshifts in the binding energy of Si 2p, as a function of the enhanced alumina content, reflected the alteration in the environment of silicon sites and progressive coating of alumina phase on the surface of the zeolite. A further increment in the alumina content to 70 wt% barely leads to further alterations in the BE value of Si 2p, which implies the dominant coating of alumina on the surface of the hierarchical zeolite.

### Dispersion state and distribution of supported Mo-oxo species within the hierarchical zeolite–alumina composite

The subsequent effect on the chemical state of Mo-oxo species was also investigated by the XPS spectra in the Mo 3d region. As

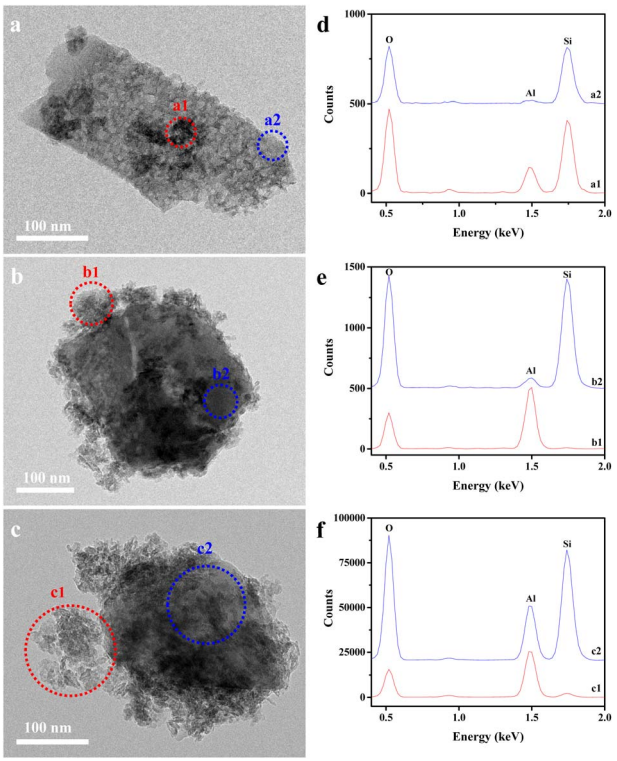


Fig. 4 TEM images and EDS spectra of (a and d) 3Mo/hZ–10Al, (b and e) 3Mo/hZ–50Al and (c and f) 3Mo/hZ–70Al catalysts.

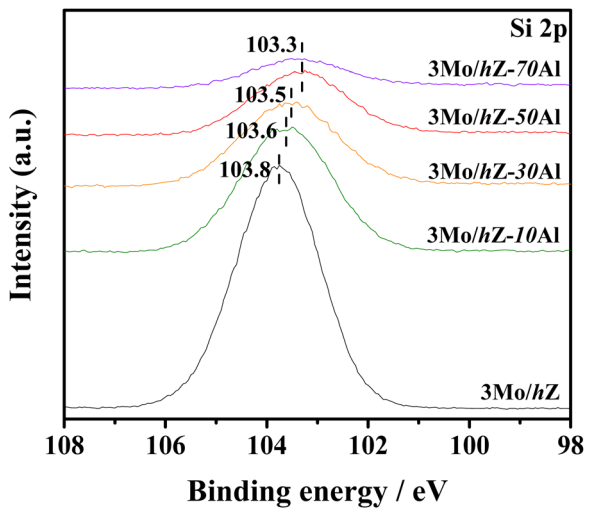


Fig. 5 Si 2p XPS spectra of 3Mo/hZ–xAl catalysts with different alumina contents.

shown in Fig. 6, the typical doublet peaks for Mo $3d_{5/2}$ (233.1 eV) and Mo $3d_{3/2}$ (236.1 eV) are displayed for 3Mo/hZ, 3Mo/hZ–10Al and 3Mo/hZ–30Al catalysts.[26,31] The stepwise broadening of the doublet of Mo 3d, as a function of enhanced alumina content, reflects the increased dispersion of molybdates.[32] When the alumina content is more than 50 wt%, the BE values of Mo 3d shift to a lower range with a decrease of about 0.4 eV for 3Mo/hZ–50Al, 3Mo/hZ–70Al and 3Mo/Al catalysts, which is related to the

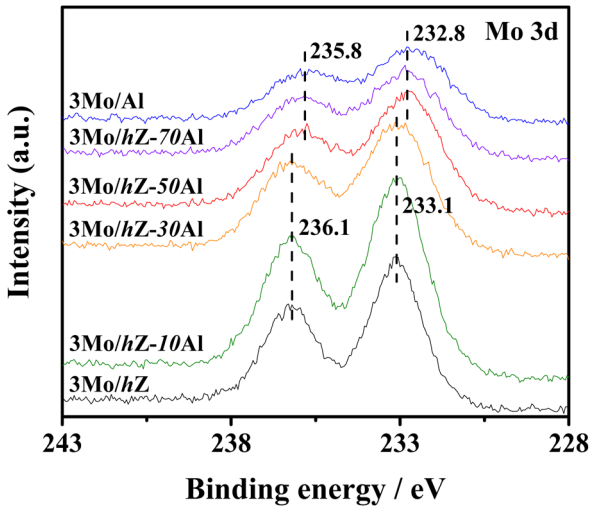


Fig. 6 Mo 3d XPS spectra of 3Mo/hZ–xAl catalysts with different alumina contents.

dominant distribution of Mo-oxo species on the alumina phase. Compared with the 3Mo/hZ catalyst, the broadening and shift of the doublet of 3Mo/Al reflect a higher level in the dispersion of molybdates,[32] and confirm the role of alumina as dispersers for the dispersion of polymolybdates into surface molybdates. The XPS results indicate the gradually increased dispersion and location of Mo-oxo species on the alumina phase of hZ–*x*Al composites along with the enhanced alumina content.

The alterations in the dispersion state and distribution of Mo-oxo species, as a function of enhanced alumina content, have been further reflected by their reducibility. As shown in Fig. 7, the $H_2$-TPR profile of 3Mo/hZ gives two main reduction peaks (833 K: initial reduction of octahedral Mo-oxo species; 938 K: deep reduction of octahedral Mo-oxo species).[33,34] After the inclusion of 10 wt% alumina into the hierarchical zeolite, two new peaks at 695 K (the initial reduction of octahedral Mo-oxo species on alumina) and 1140 K (deep/complete reduction of tetrahedral and octahedral Mo-oxo species on alumina) appear at the 3Mo/hZ–10Al.[33,34] With the enhancement of alumina content, the main peaks at 833 K and 938 K turn into the satellites peaks for 3Mo/hZ–30Al and become indiscernible for 3Mo/hZ–50Al. The $H_2$-TPR profiles of 3Mo/hZ–50Al, 3Mo/hZ–70Al, 3Mo/hZ–90Al and comparative 3Mo/Al show analogous shape and position of main characteristic peaks, which refers to the similar dispersion situation of Mo-oxo species and the dominant distribution of these Mo-oxo species on the alumina.

### Discussion of the effect of alumina content on the metathesis activity

The well-known composition effect of zeolite by the introduction of alumina is usually focused on the improved mechanistic strength and thermal stability. Our previous investigation discloses the synergetic effect between zeolites and alumina for the achievement of active metathesis catalysts, in which alumina plays as the disperser and the zeolite plays as the anchorages for active sites, respectively.[24,28] In this case, the

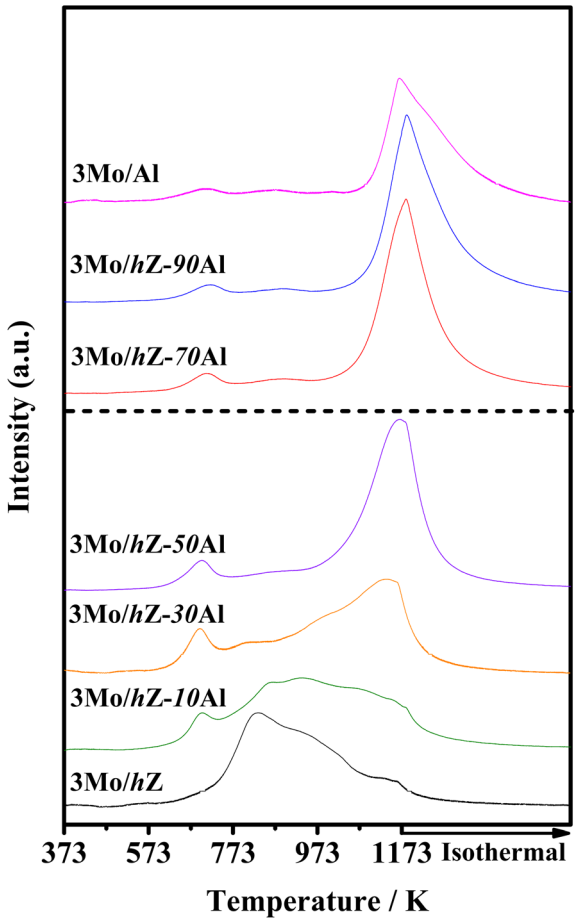


Fig. 7 $H_2$-TPR profiles of 3Mo/hZ–*x*Al catalysts with different alumina contents.

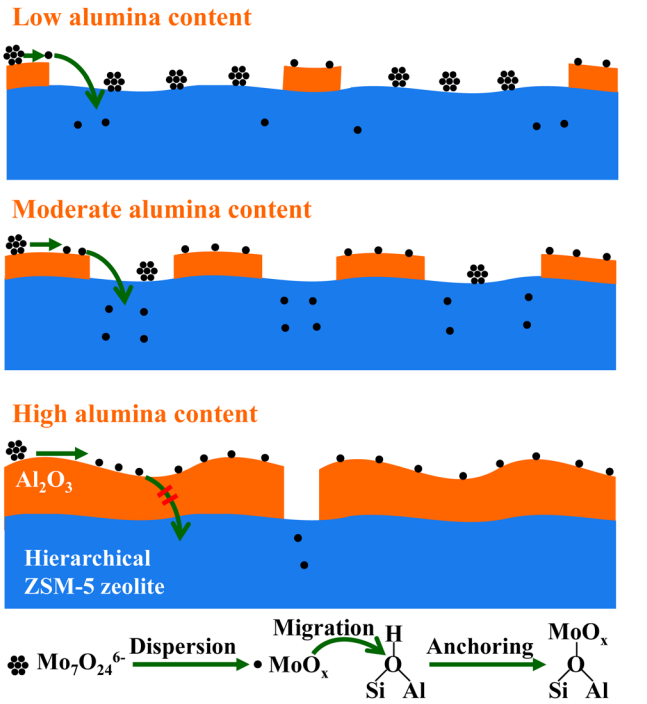


Scheme 2 Schematic description of the effect of alumina content on the preparation of active metathesis catalysts.

composition of hierarchical zeolites and alumina is also essential for the preparation of active Mo-based catalysts for the cross-metathesis between ethene and 2-butene, depending on the interaction mode between hierarchical ZSM-5 zeolite and alumina. The underlying fundamental understanding is depicted in Scheme 2.

In the case of low alumina content, the dispersion of supported Mo-oxo species is hampered due to the sparse distribution of interacted alumina–zeolite, which disables the beginning of the transformation of active sites. Upon the moderate enhancement of alumina content to 30 wt%, the desirable interaction mode between the hierarchical zeolite and alumina ensures the dispersion of Mo-oxo species and also enables the subsequent transportation of dispersed Mo-oxo species from alumina to hierarchical zeolite, *i.e.* the anchoring of dispersed Mo-oxo species on Brønsted acid sites in zeolite micropores. Upon the excessive alumina content in composites, the coating and enveloping of alumina on the surface of zeolites dominate the interaction mode of hierarchical zeolites and alumina. In such case, the supported Mo-oxo species mainly distribute on the surface of alumina phase, and the migration/penetration of Mo-oxo species is hampered by the thick layers of alumina. Therefore, the synergetic effect between zeolites and alumina no longer works well for the generation of active sites. As a result, with the enhancement of alumina content in the range of 50–90 wt%, the metathesis activity of composite catalysts gradually drops to that of $MoO_3/Al_2O_3$ (3Mo/Al).

## Conclusions

In summary, the significant impact of composition of hierarchical ZSM-5 zeolite–alumina composites on the supported Mo-based catalysts has been demonstrated in the cross-metathesis reaction between ethene and 2-butene. The ethene conversion increases from 24.1% to 49.2% with the increase in the alumina content in composites from 10 wt% to 30 wt%. A further increase in the alumina content leads to reduced metathesis activity, in which the ethene conversion decreases from 30.3% to 4.8% upon the enhanced alumina content from 50 wt% to 90 wt%. Such tendency is closely associated with the interaction mode between the hierarchical ZSM-5 zeolite and alumina. TEM observation as well as EDS analysis and XPS results indicate the progressive coating and enveloping of alumina phase on the surface of the hierarchical ZSM-5 zeolite along with the enhanced alumina content. The desired interaction mode, as a result of moderate alumina content, enables the dispersion of supported Mo-oxo species and subsequent transportation into zeolite micropores, which thus enables the preparation of active metathesis catalysts.

## Author contributions

Ning Wei: methodology, data acquisition, experiments, writing. Weiping Zhang: experimental discussion, formal analysis,

writing, supervision. Dazhi Zhang: data acquisition. Shengjun Huang: experimental discussion, formal analysis, writing, funding, supervision.

## Conflicts of interest

There are no conflicts to declare.

## Acknowledgements

This work was supported by Natural Science Foundation of China (No. 21776272), Dalian Bureau of Science and Technology (No. 2020JJ25CY007) and CenerTech Tianjin Chemical Research and Design Institute (Co., Ltd.).

## Notes and references

1 A. Primo and H. Garcia, *Chem. Soc. Rev.*, 2014, **43**, 7548.
2 W. Vermeiren and J.-P. Gilson, *Top. Catal.*, 2009, **52**, 1131.
3 Y. H. Hou, S. Ogasawara, A. Fukuoka and H. Kobayashi, *Catal. Sci. Technol.*, 2017, **7**, 6132.
4 X. Zeng, Z. C. Wang, J. Ding, L. Z. Wang, Y. J. Jiang, C. Stampfl, M. Hunger and J. Huang, *J. Catal.*, 2019, **380**, 9.
5 Q. M. Sun, N. Wang and J. H. Yu, *Adv. Mater.*, 2021, **33**, 2104442.
6 E. T. C. Vogt and B. M. Weckhuysen, *Chem. Soc. Rev.*, 2015, **44**, 7342.
7 S. Mitchell, N. L. Michels and J. Perez-Ramirez, *Chem. Soc. Rev.*, 2013, **42**, 6094.
8 K. Y. Yang, D. Z. Zhang, M. M. Zou, L. L. Yu and S. J. Huang, *ChemCatChem*, 2021, **13**, 1414.
9 S. P. Verkleij, G. T. Whiting, S. P. Esclapez, M. M. Mertens, A.-J. Bons, M. Burgers and B. M. Weckhuysen, *Catal. Sci. Technol.*, 2018, **8**, 2175.
10 G. T. Whiting, F. Meirer, M. M. Mertens, A. J. Bons, B. M. Weiss, P. A. Stevens, E. de Smit and B. M. Weckhuysen, *ChemCatChem*, 2015, **7**, 1312.
11 G. T. Whiting, F. Meirer, D. Valencia, M. M. Mertens, A.-J. Bons, B. M. Weiss, P. A. Stevens, E. de Smit and B. M. Weckhuysen, *Phys. Chem. Chem. Phys.*, 2014, **16**, 21531.
12 L. Lakiss, C. Kouvatas, J.-P. Gilson, V. Valtchev, S. Mintova, C. Fernandez, R. Bedard, S. Abdo and J. Bricker, *J. Phys. Chem. C*, 2021, **125**, 20028.
13 M. W. Kasture, P. S. Niphadkar, V. V. Bokade and P. N. Joshi, *Catal. Commun.*, 2007, **8**, 1003.
14 K. Cheng, L. C. J. Smulders, L. I. v. d. Wal, J. Oenema, J. D. Meeldijk, N. L. Visser, G. Sunley, T. Roberts, Z. Xu, E. Doskocil, H. Yoshida, Y. Zheng, J. Zečević, P. E. de Jongh and K. P. de Jong, *Science*, 2022, **377**, 204.
15 K. Cheng, L. I. van der Wal, H. Yoshida, J. Oenema, J. Harmel, Z. R. Zhang, G. Sunley, J. Zecevic and K. P. de Jong, *Angew. Chem., Int. Ed.*, 2020, **59**, 3592.
16 G. T. Whiting, S. H. Chung, D. Stosic, A. D. Chowdhury, L. I. van der Wal, D. L. Fu, J. Zecevic, A. Travert, K. Houben, M. Baldus and B. M. Weckhuysen, *ACS Catal.*, 2019, **9**, 4792.
17 G. T. Whiting, N. Nikolopoulos, I. Nikolopoulos, A. D. Chowdhury and B. M. Weckhuysen, *Nat. Chem.*, 2019, **11**, 23.
18 S. Mitchell, N.-L. Michels, K. Kunze and J. Pérez-Ramírez, *Nat. Chem.*, 2012, **4**, 825.
19 J. S. J. Hargreaves and A. L. Munnoch, *Catal. Sci. Technol.*, 2013, **3**, 1165.
20 T. Shoinkhorova, A. Dikhtiarenko, A. Ramirez, A. Dutta Chowdhury, M. Caglayan, J. Vittenet, A. Bendjeriou-Sedjerari, O. S. Ali, I. Morales-Osorio, W. Xu and J. Gascon, *ACS Appl. Mater. Interfaces*, 2019, **11**, 44133.
21 S. A. Bradley, X. Luo, J. He, T. H. Chao and R. D. Gillespie, *Catal. Lett.*, 1997, **47**, 205.
22 J. Zecevic, G. Vanbutsele, K. P. de Jong and J. A. Martens, *Nature*, 2015, **528**, 245.
23 Z. Vajglová, N. Kumar, M. Peurla, J. Peltonen, I. Heinmaa and D. Y. Murzin, *Catal. Sci. Technol.*, 2018, **8**, 6150.
24 S. J. Huang, F. C. Chen, S. L. Liu, Q. J. Zhu, X. X. Zhu, W. J. Xin, Z. C. Feng, C. Li, Q. X. Wang and L. Y. Xu, *J. Mol. Catal. A: Chem.*, 2007, **267**, 224.
25 S. J. Huang, S. L. Liu, W. J. Xin, J. Bai, S. J. Xie, Q. X. Wang and L. Y. Xu, *J. Mol. Catal. A: Chem.*, 2005, **226**, 61.
26 S. J. Huang, H. J. Liu, L. Zhang, S. L. Liu, W. J. Xin, X. J. Li, S. J. Xie and L. Y. Xu, *Appl. Catal., A*, 2011, **404**, 113.
27 S. J. Huang, S. L. Liu, Q. J. Zhu, X. X. Zhu, W. J. Xin, H. J. Liu, Z. C. Feng, C. Li, S. J. Xie, Q. X. Wang and L. Y. Xu, *Appl. Catal., A*, 2007, **323**, 94.
28 N. Wei, L. Z. Wang, W. J. Yang, D. Z. Zhang, Z. H. Jia, W. Liu, W. P. Zhang, J. Z. Zang, S. J. Huang and J. Huang, *Chem.–Eur. J.*, 2023, DOI: **10.1002/chem.202300543**.
29 D. Chichova, P. Maki-Arvela, T. Heikkila, N. Kumar, J. Vayrynen, T. Salmi and D. Y. Murzin, *Top. Catal.*, 2009, **52**, 359.
30 L. Ferreira, A. M. Fonseca, G. Botelho, C. Almeida-Aguiar and I. C. Neves, *Microporous Mesoporous Mater.*, 2012, **160**, 126.
31 Y. V. Plyuto, I. V. Babich, I. V. Plyuto, A. D. VanLangeveld and J. A. Moulijn, *Appl. Surf. Sci.*, 1997, **119**, 11.
32 N. K. Nag, *J. Phys. Chem.*, 1987, **91**, 2324.
33 S. Rajagopal, H. J. Marini, J. A. Marzari and R. Miranda, *J. Catal.*, 1994, **147**, 417.
34 V. O. O. Goncalves, C. Ciotonea, S. Arrii-Clacens, N. Guignard, C. Roudaut, J. Rousseau, J. M. Clacens, S. Royer and F. Richard, *Appl. Catal., B*, 2017, **214**, 57.